



Contents lists available at ScienceDirect

# Journal of the Mechanical Behavior of Biomedical Materials

journal homepage: [www.elsevier.com/locate/jmbbm](http://www.elsevier.com/locate/jmbbm)

## Analyzing nature's protective design: The glyptodont body armor

Anton du Plessis<sup>a,\*</sup>, Chris Broeckhoven<sup>b</sup>, Igor Yadroitsev<sup>c</sup>, Ina Yadroitsava<sup>c</sup>,  
Stephan Gerhard le Roux<sup>a</sup>

<sup>a</sup> CT Scanner Facility, Central Analytical Facilities, Stellenbosch University, Matieland, 7602 Stellenbosch, South Africa

<sup>b</sup> Laboratory of Functional Morphology, Department of Biology, University of Antwerp, Wilrijk 2610, Belgium

<sup>c</sup> Department of Mechanical and Mechatronic Engineering, Central University of Technology, Bloemfontein 9300, South Africa

### ARTICLE INFO

#### Keywords:

Biomimicry  
Osteoderm  
Micro-computed tomography  
Reverse-engineering, stress simulation

### ABSTRACT

Many animal species evolved some form of body armor, such as scales of fish and bony plates or osteoderms of reptiles. Although a protective function is often taken for granted, recent studies show that body armor might comprise multiple functionalities and is shaped by trade-offs among these functionalities. Hence, despite the fact that natural body armor might serve as bio-inspiration for the development of artificial protective materials, focussing on model systems in which body armor serves a solely protective function might be pivotal. In this study, we investigate the osteoderms of *Glyptotherium arizonae*, an extinct armadillo-like mammal in which body armor evolved as protection against predators and/or tail club blows of conspecifics. By using a combination of micro-computed tomography, reverse-engineering, stress simulations and mechanical testing of 3D printed models, we show that the combination of dense compact layers and porous lattice core might provide an optimized combination of strength and high energy absorption.

### 1. Introduction

Various forms of protective body armor are present in the animal kingdom, including the scales of fish and pangolins, the carapaces of turtles and osteoderms - bony plates embedded in the skin of crocodiles and armadillos (Yang et al., 2012, 2013). Natural body armor comes in many shapes, ranging from overlapping, highly-flexible elements (Yang et al., 2012, 2013) to rigid hexagonal structures interlocked with sutures (Yang et al., 2015). The diversity in structure and associated mechanical behavior has made natural body armor a promising candidate for the bio-inspiration of artificial protective materials (Yang et al., 2012, 2013; Chintapalli et al., 2014; Naleway et al., 2015; Wang et al., 2016; Torres and Lama, 2017). However, recent studies show that natural body armor might not only fulfil a protective role, but is instead shaped by multiple selective pressures (Broeckhoven et al., 2017). For example, Broeckhoven et al. (2017) demonstrate a functional trade-off between strength and thermal capacity of osteoderms in two species of girdled lizards. Hence, appropriate selection of model systems for the bio-inspiration of artificial body armor, i.e. those that serve a (almost) solely protective function, is pivotal for the advancement of protective materials.

Glyptodonts or glyptodontines (Fig. 1) are extinct mammals belonging to the order Cingulata, which includes modern-day armadillos (Delsuc et al., 2016). They roamed the American continent from the

Miocene to Pleistocene, but went extinct some 10,000 years ago. Many glyptodonts were large, up to size of a small car, and possessed a solid protective carapace consisting of interlocking osteoderms. The carapace of glyptodonts was relatively rigid, unlike the more flexible organization present in armadillos (Chen et al., 2011). It has been proposed that the armor of glyptodonts evolved either to resist attacks by large co-occurring predators, or more plausible, serve as protection against the powerful tail-blows of conspecifics during intraspecific fights (Alexander et al., 1999; Blanco et al., 2009; Arbour and Zanno, 2018). Unlike reptiles, these mammals did not require thermal regulation, eliminating this role for the dermal armor. Yet, despite its (presumably) sole protective function, the mechanical behavior of glyptodont osteoderms has never been investigated.

In this study, we examine the mechanical behavior of glyptodont osteoderms, with particular focus on the structural parameters that might be crucial to its protective function. To do so, we employ a combination of micro-computed tomography techniques, computer simulation and mechanical testing, using reverse-engineered osteoderms produced by additive manufacturing. By analyzing the compressive behavior and energy absorption capabilities of the glyptodont osteoderms, we aim to provide a better understanding of the configuration required for carrying out a protective function, which ultimately can serve to improve the bio-inspiration of artificial body armor.

\* Corresponding author.

E-mail address: [anton2@sun.ac.za](mailto:anton2@sun.ac.za) (A. du Plessis).



Fig. 1. Left: photograph of a fossil reconstruction of a glyptodont (here: *Panochthus frenzelianus*) showing its body armor consisting of interlocking osteoderms. Top right: photograph of an isolated *Glyptotherium arizonae* osteoderm used in this study. Bottom right: three-dimensionally rendered micro-CT image of the isolated osteoderm showing the compact layers surrounding the cancellous core.

## 2. Methods

### 2.1. Micro-computed tomography and reverse engineering of osteoderms

An isolated osteoderm of *Glyptotherium arizonae* was purchased from a commercial dealer (Prehistoric Florida, Tallahassee, FL) and microCT scanned at high resolution using a GE Phoenix v|tome|x L240 dual tube CT instrument (Phoenix X-ray; General Electric Sensing & Technologies, Wunstorf, Germany) located at the Stellenbosch micro-CT facility (Du Plessis et al., 2016). Following the guidelines in Du Plessis et al. (2017a), micro-CT scanning was conducted at 120 kV, 100  $\mu$ A and with a voxel size of 30  $\mu$ m. Data analysis was performed in Volume Graphics VGStudioMax 3.0. Simplified reverse engineered models were created based on the morphological measurements taken from micro-CT data. The models with lattice structures were created in the software Materialise Magics, including the lattice structure module. Models were produced with EOSINT P380 laser sintering system using PA2200 polyamide powder.

### 2.2. Computer simulations and mechanical testing

Static load simulation was performed using a direct voxel-based structural mechanics simulation module (see Broeckhoven et al., 2017; Broeckhoven and du Plessis, 2017; Du Plessis et al., 2017b, 2018). Simulations were performed assuming homogenous, elastic material properties. The base was kept fixed and a 1 kN load was applied to a 2 mm diameter circular area on the top surface, using Ti6Al4V material

properties. This material was selected as it is particularly well suited to additive manufacturing of bio-inspired models. All simulation results were compared relative to one another only, therefore the conclusions made from these simulation results are valid for all materials in the linear elastic regime. However, in this work the testing was conducted with polymer printed models, due to limitations in the maximum compressive force of the available test equipment. Mechanical tests were conducted using a universal test machine (Model 43, MTS, 30 kN maximum force). Compression testing was performed at 1.5 mm per second. Absorption energy was calculated from the obtained stress-strain data according to the procedures in Maskery et al. (2017) and originally in Gibson and Ashby (1999). Of each different design variation, stress-strain curves were obtained for 3 replicates.

## 3. Results and discussion

### 3.1. Morphological analysis and reverse engineering

Osteoderms of *Glyptotherium arizonae* consist of a cancellous trabecular core sandwiched between two compact layers. Each hexagonal osteoderm is joined to the adjacent osteoderms with sutures, thereby making a rigid shield or carapace, as seen in other natural body armor (Chen et al., 2011, 2015; Yang et al., 2015; Achrai and Wagner, 2017). A three-dimensionally rendered image of an osteoderm micro-CT scan is shown in Fig. 1. Several quantitative measurements were obtained from the micro-CT scan, including the thickness of the compact layer, the mean strut thickness of the cancellous core, and the total porosity of the cancellous core. An internal rectangular region-of-interest (ROI), measuring  $10 \times 10 \times 4$  mm, was digitally extracted from the micro-CT scan and was used to characterize the cancellous core in subsequent analyses (Fig. 2). Total porosity was measured using basic morphological tools. Strut thickness measurement was performed using the maximal-spheres method to find the actual thickness at every point in the structure, thereby producing a strut thickness distribution from which we obtained a mean value (Fig. 2). Total porosity of this internal ROI was 66%, whereas the mean strut thickness was 0.25 mm. These values, in combination with basic dimensional measurements and measurement of the total porosity of the entire osteoderm including the sides, were then used to determine parameters for a reverse-engineered simplified model with surrounding compact layers and lattice core. All measurements including those used for the reserve-engineered model are shown in Table 1.

Our simplified reverse-engineered model consisted of a hexagonal shape with 1 mm thick compact outer layer and contained a regular strut-based diamond-design lattice with total lattice porosity of 80% and unit cell 1.5 mm (which results in strut thickness 0.31 mm). In this design, the cancellous core has a similar strut thickness, but in total a

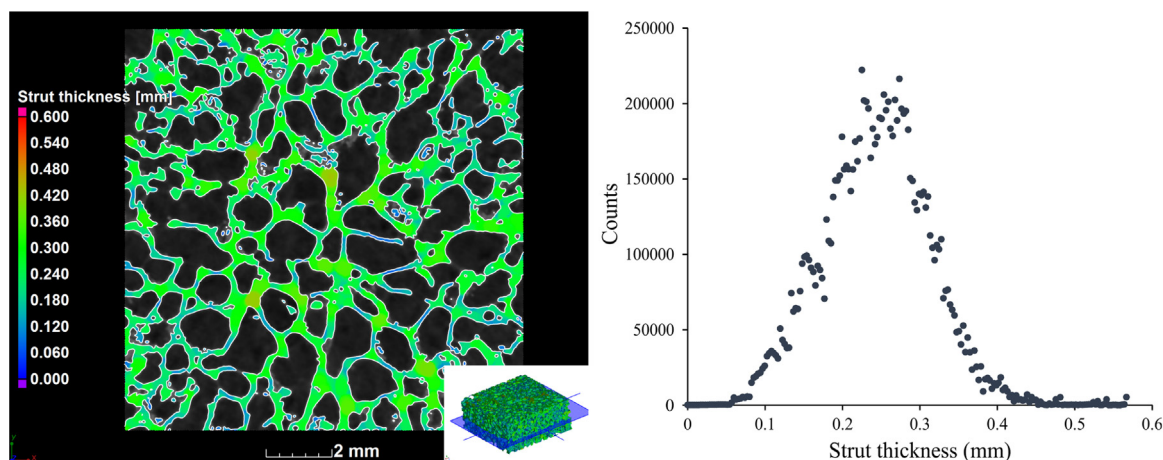


Fig. 2. Slice view of the cancellous core of the osteoderm (left) and its strut thickness distribution (right).

**Table 1**  
Dimensions of the *Glyptotherium* osteoderm used for micro-CT analysis and of the reverse-engineered model.

	Osteoderm	Model
Max width (mm)	28	28
Height (mm)	12	12
Total porosity (%)	56	56
Porosity of foam core (%)	66	80
Foam core strut thickness (mm)	0.25	0.31

slightly higher porosity than that of the actual osteoderm. This is due to the fact that the sides and compact layers of the actual osteoderm contain some degree of porosity, resulting in a total porosity of 56%. In order to obtain the same total porosity, the reverse-engineered model required a more porous core, in combination with its solid sides. A comparison of the actual and reverse-engineered osteoderms is shown in Fig. 3.

### 3.2. Stress simulations

Static load simulations (linear elastic isotropic medium assumption) on the reverse-engineered model allowed for the assessment of the effects of changes in design parameters on the mechanical properties (here: stress distribution) of the structure. An example hereof is shown in Fig. 4, with the red areas highlighting the highest von Mises stress. Here, we varied several design parameters, including strut thickness and thickness of the compact layers, as well as changes in load conditions, to unravel the unique properties of these natural ‘sandwich structures’.

#### 3.2.1. Load area size and angle

The size of the load application and the angle at which the load was applied, was investigated. Smaller load areas, corresponding to sharper objects, cause increasingly higher stresses for a given force (see Fig. 5a). This can be understood as the natural structure evolved to withstand blunt impact from large objects such as tail-clubs and not as protection against sharp objects such as teeth.

Another possible advantage of a sandwich structure is the ability of the compact layer to distribute the stress and minimize the effect of load angle changes. Changing the angle of the load to 45 degrees slightly reduced the maximum von Mises stress (Fig. 5b). This can be explained by the fact that the compact layer is absorbing more load at an angle when compared to a perpendicular load.

#### 3.2.2. Strut thickness variation

Investigating changes in the strut thickness of the internal lattice was performed in two ways. In the first method, this was achieved by thickening the struts directly in the lattice unit cell, which also changed the total porosity of the structure (a thicker strut results in total higher density). The mechanical properties of lattices and open-cell foams are directly related to the total porosity as described by Gibson and Ashby (1999). Therefore as expected, thicker struts distribute stress better: since the effective density of the structure is higher, the stress is distributed over a larger material fraction resulting in lower stress for thicker struts (Fig. 5c). However, it is expected that as the density continues to increase (i.e., overall structure becomes more compact), the failure becomes more catastrophic. Consequently, there should be a trade-off between strength and strut thickness (or overall density) to maximize impact resistance without the risk of catastrophic failure.

#### 3.2.3. Unit cell size change

Changing the strut thickness is also possible without a density change, when changing the unit cell size (in contrast to the above method of strut thickness change with density change). When the unit cell size is increased, the strut thickness increases but the number of struts in the same volume reduces, which leaves the total density unchanged. A series of simulations for three unit cell sizes of the internal lattice in the reverse-engineered model were performed. Our results show that unit cell size does not affect the maximum von Mises stress (Fig. 5d). This indicates that more thinner struts are equivalent to less thicker struts. This is limited, in practice, to the minimum feature size that can be produced by additive manufacturing. The smallest unit cell size and hence strut thickness that can be manufactured is typically limited to about 0.15 mm, depending on the system used. However, as a

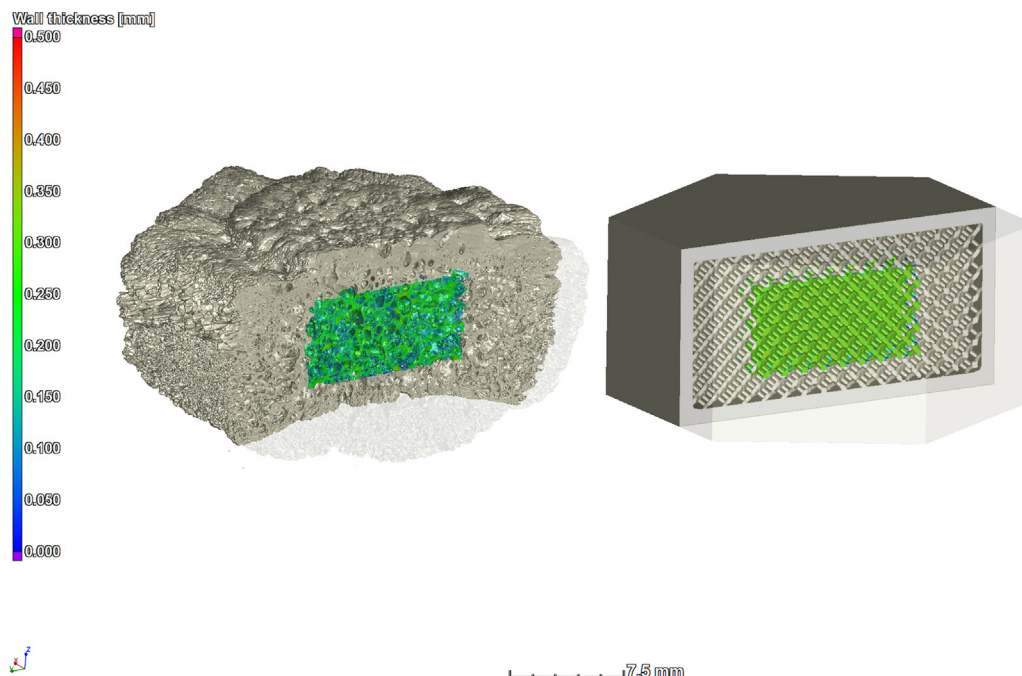


**Fig. 3.** Image illustrating the similarity in strut thickness between the osteoderm (left) and simplified reverse-engineered model (right).

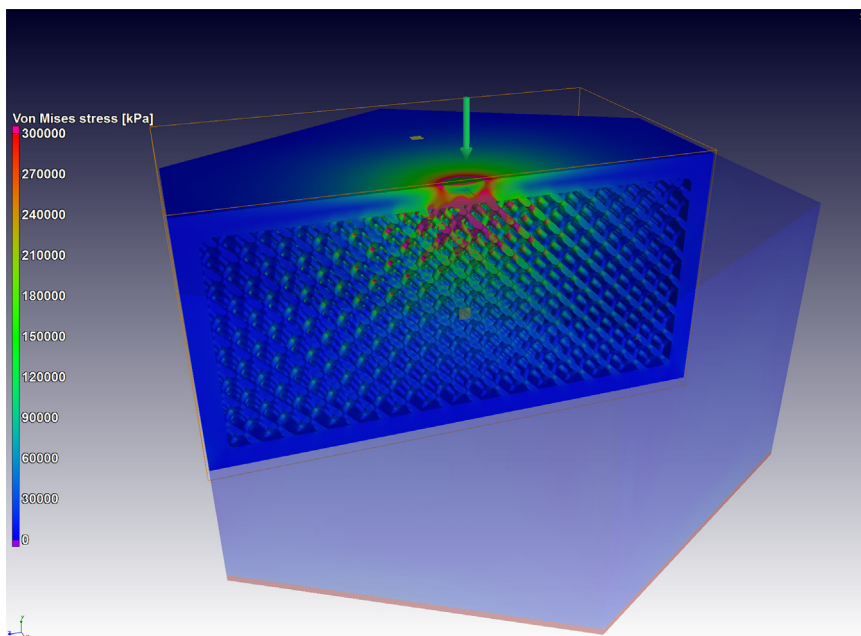


Fig. 4. Load simulation result showing the maximum von Mises stress distribution in the reverse engineered model after applying a 2 mm diameter load to the top surface.

protective material, more thin struts are preferred as the likelihood of catastrophic failure is reduced – if one strut fails there are many that still carry load when using thinner struts.

### 3.2.4. Presence of compact layers

To investigate the effect of the removal of the compact layers, simulations were performed on identical samples with and without compact layers. Removal of the compact layers resulted in an almost three-fold increase in maximum von Mises stress (Fig. 5e), highlighting

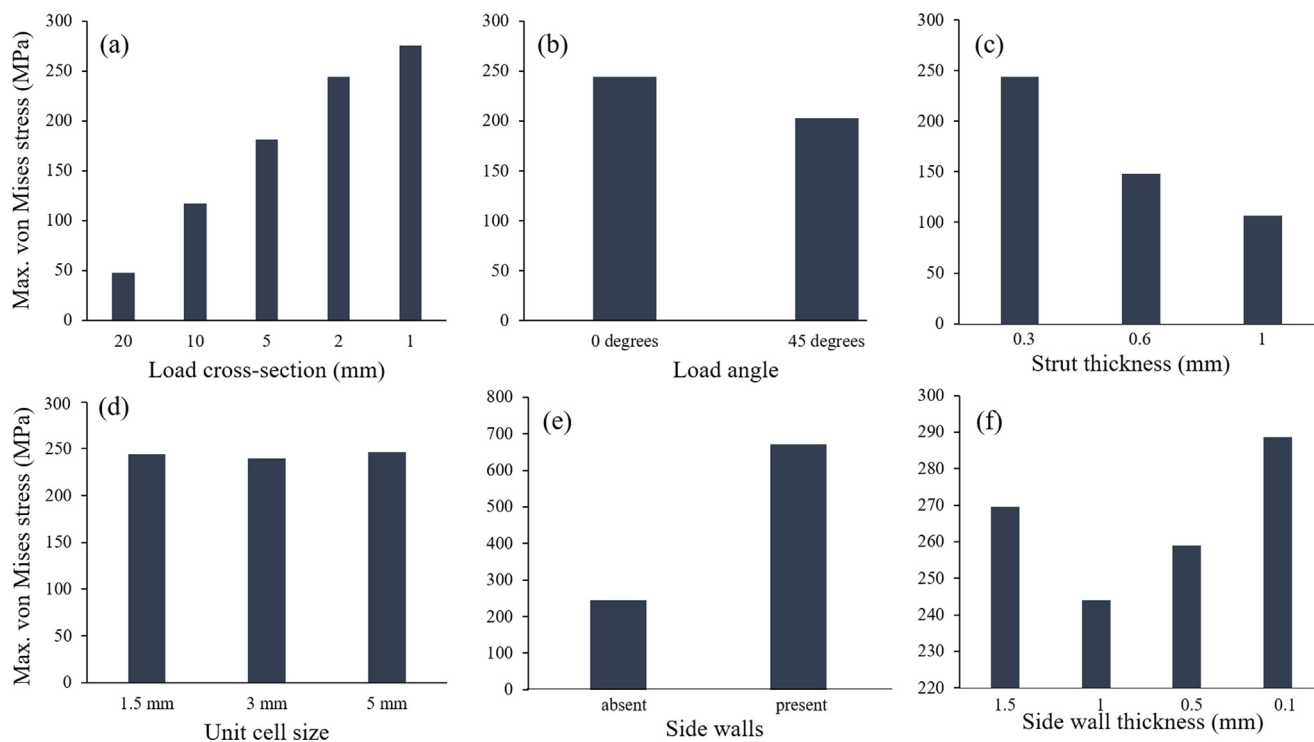


Fig. 5. Results of static load simulations on a reverse-engineered model of a *Glyptotherium* osteoderm. a, the effect of load area size change on the maximum von Mises stress; b, comparison of maximum von Mises stress between perpendicular load and a 45-degree load for 2 mm cross-sectional load area; c, effect of strut thickness change in combination with density change (i.e., 80%, 63% and 43% porosity, respectively); d, effect of unit cell size in combination with strut thickness change (i.e., 0.3 mm, 0.6 mm and 1.0 mm strut thickness, respectively); e, maximum von Mises stress for models with and without side walls; f, effect of varying side wall thickness while keeping the total porosity constant (internal strut thickness changed to compensate for side wall thickness change).

the importance of the compact layers, especially dorsally, in distributing the stress upon impact and limiting damage to the structure.

### 3.2.5. Thickness of compact layers

The compact layers and their thickness appear to have a major influence on the mechanical properties of the structure. To isolate the effect of the compact layer, we varied the thickness thereof and changed the internal lattice porosity accordingly: as the thickness of the compact layer increased, a lower porosity lattice core was incorporated to keep the total porosity of the model reasonably constant. Simulations were run using models with wall thicknesses of 0.1 mm, 0.5 mm, 1 mm and 1.5 mm. In each case the internal lattice was changed to match the total density of the structure, i.e. a thick-wall structure has very high internal porosity and hence lacks internal support, while a very thin wall design has very thick internal lattice struts. The results of our simulations indicate that the reverse engineered structure might be biomechanically optimized – it has a lower stress value at 1 mm compared to thinner or thicker walls (Fig. 5f). On the one hand, thick side walls might cause high stress values locally in the lattice or the upper layer itself where load is applied - due to lack of sufficient internal support. On the other hand, thin side walls might cause higher stress values on the struts themselves: the side walls do not carry any of the load in this case and all the load is carried by the struts. In this geometry, for a 28 mm-diameter and 12 mm height hexagon, the optimal shell thickness is near 1 mm.

### 3.3. Mechanical testing and energy absorption

Firstly, we tested the effect of variation in lattice density while keeping the thickness of the compact layer constant. As expected, a denser sample has a higher yield strength and a steeper stress increase after yielding. As the sample density reduces, the yield stress reduces (Fig. 6). Secondly, we examined the role of the compact layer surrounding the cancellous core. The reverse-engineered model without a

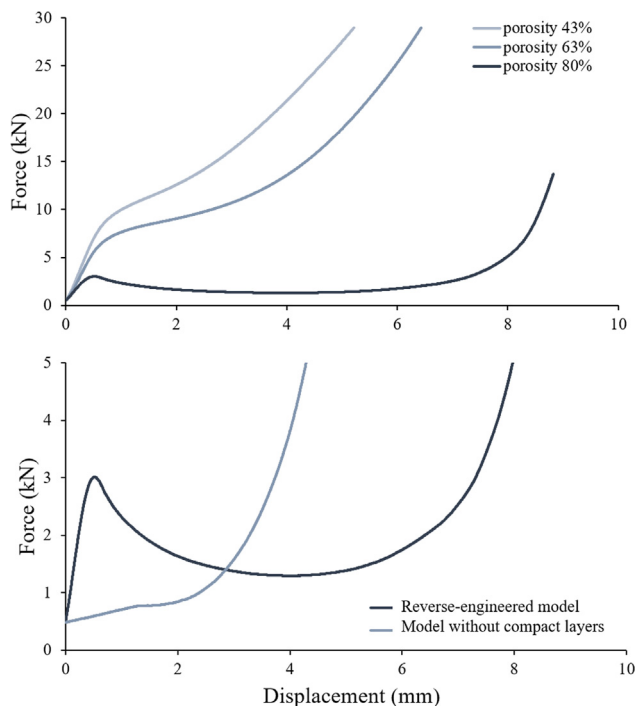


Fig. 6. Top: stress-strain data obtained from compression of reverse-engineered samples with varying lattice porosity (i.e., 43%, 62%, 80% porosity of the internal lattice, respectively). Bottom: comparison of stress-strain curves for samples with and without compact layers.

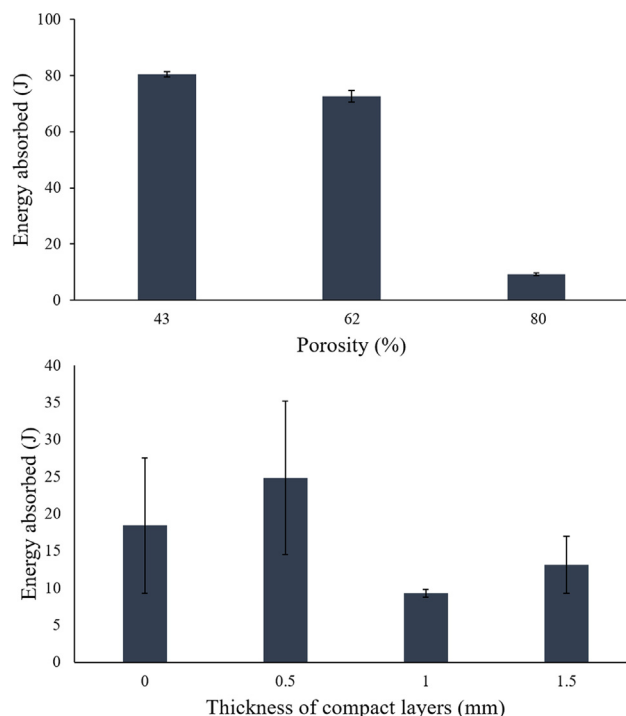


Fig. 7. Energy absorption for different lattice density (top), and for samples with varying compact layer thickness (bottom). The average value (i.e., mean of the three replicates)  $\pm$  standard deviations are shown.

compact layer has no yield strength and continuously yields up to full densification, whereas the model with compact layers has a higher yield strength and then a plateau region before final densification. The above-mentioned results indicate that the internal lattice plays an important role in the strength of the structure, with a denser lattice being stronger for both initial yield strength, as well as strength after yielding, for the polymer material used in the tests. The role of the compact layers is therefore shown to be crucial to provide initial yield strength, i.e., it provides protection against initial yielding.

Next, we calculated the energy absorption for deformation up to 25% from initial sample height for the compression tests. Our results show that lower porosity, as well as the presence of the compact layer increases the energy absorption (Fig. 7). As the internal lattice becomes denser, the protective role increases based on total energy absorption and strength, but it is expected that its yielding behavior will become more catastrophic (depending on the material ductility). As the shell thickness increases from 0 to 0.5 mm, the energy absorption increases as expected due to the protective role of the shell and the combined effect of the lattice and shell. As the shell increases in thickness to 1 mm, the lattice struts become thinner and more difficult to manufacture accurately, resulting in reduced energy absorption. As the shell thickness increases to 1.5 mm, at which point it does not contain any internal supports, the energy absorption increases but the failure is catastrophic. This series of experiments demonstrates the compromise between the unique combination of compact layers and lattice core, providing a protective role. It must be noted that in these experiments, a polymer material was used, which is more ductile than bone. In the case of real osteoderms, a lower-density core is required to prevent brittle and catastrophic failure of the bone material. While a polymer material was used for these experiments, this work demonstrates a general biomimetic approach to designing an impact protective geometry using additive manufacturing, which can be applied to any material. Future work using Ti6Al4V is planned which will further demonstrate the methodology. Due to its biomedical relevance, additive manufacturing of Ti6Al4V has been extensively investigated and optimized to the point where today almost defect-free production of

complex geometries are possible. Ceramics are used widely in impact protective devices but current additive manufacturing of ceramics are limited by maximum size, microporosity and other defects, hence this might be useful in the future once these limitations have been solved.

#### 4. Conclusions

Osteoderms of an extinct glyptodont were analyzed using high resolution micro-CT, simulations and mechanical testing of reverse-engineered models with varying morphological parameters. Our results show that the combination of dense compact layers and a porous lattice core contribute to the strength of the structure and the prevention of catastrophic failure. These findings suggest that the osteoderms of *Glyptotherium* might be biomechanically optimized structures. It is envisaged that this study assists in the search for optimal protective designs to be used in future additively manufactured protective materials.

#### Acknowledgements

Materialise is acknowledged for providing a temporary license of Magics with the structures module, which was used for model and lattice generation. We thank Johan Els and Andre Heydenrych of the Centre for Rapid Prototyping and Manufacturing (CRPM, CUT), for providing 3D print services for the physical models. We thank Dean Koupryanoff for his assistance with mechanical testing.

#### References

- Achrai, B., Wagner, H.D., 2017. The turtle carapace as an optimized multi-scale biological composite armor – a review. *J. Mech. Behav. Biomed. Mater.* 73, 50–67.
- Alexander, R.M., Fraiña, R.A., Vizcaíno, S.F., 1999. Tail blow energy and carapace fractures in a large glyptodont (Mammalia, Xenarthra). *Zool. J. Linn. Soc.* 126, 41–49.
- Arbour, V.M., Zanno, L.E., 2018. The evolution of tail weaponization in amniotes. *Proc. R. Soc. Lond. B Biol. Sci.* 285, 20172299.
- Blanco, R.E., Jones, W.W., Rinderknecht, A., 2009. The sweet spot of a biological hammer: the centre of percussion of glyptodont (Mammalia: Xenarthra) tail clubs. *Proc. R. Soc. Lond. B Biol. Sci.* 276, 3971–3978.
- Broeckhoven, C., du Plessis, A., 2017. Has snake fang evolution lost its bite? New insights from a structural mechanics viewpoint. *Biol. Lett.* 13, 20170293.
- Broeckhoven, C., du Plessis, A., Hui, C., 2017. Functional trade-off between strength and thermal capacity of dermal armor: insights from girdled lizards. *J. Mech. Behav. Biomed. Mater.* 74, 189–194.
- Chen, I.H., Kiang, J.H., Correa, V., Lopez, M.I., Chen, P.-Y., McKittrick, J., Meyers, M.A., 2011. Armadillo armor: mechanical testing and micro-structural evaluation. *J. Mech. Behav. Biomed. Mater.* 4, 713–722.
- Chen, I.H., Yang, W., Meyers, M.A., 2015. Leatherback sea turtle shell: a tough and flexible biological design. *Acta Biomater.* 28, 2–12.
- Chintapalli, R.K., Mirkhalaf, M., Dastjerdi, A.K., Barthelat, F., 2014. Fabrication, testing and modeling of a new flexible armor inspired from natural fish scales and osteoderms. *Bioinspiration Biomim.* 9, 036005.
- Delsuc, F., Gibb, G.C., Kuch, M., Billet, G., Hautier, L., Southon, J., Rouillard, J.M., Fericola, J.C., Vizcaíno, S.F., MacPhee, R.D., Poinar, H.N., 2016. The phylogenetic affinities of the extinct glyptodonts. *Curr. Biol.* 26, R155–R156.
- Du Plessis, A., le Roux, S.G., Guelpa, A., 2016. The CT scanner facility at Stellenbosch University: an open access X-ray computed tomography laboratory. *Nucl. Instrum. Methods Phys. Res. Sect. B Beam Interact. Mater. At.* 384, 42–49.
- Du Plessis, A., Broeckhoven, C., le Roux, S.G., 2018. Snake fangs: 3D morphological and mechanical analysis by microCT, simulation and physical compression testing. *GigaScience* 7, 1–8.
- Du Plessis, A., Broeckhoven, C., Guelpa, A., le Roux, S.G., 2017a. Laboratory X-ray micro-computed tomography: a user guideline for biological samples. *GigaScience* 6, 1–11.
- Du Plessis, A., Yadroitsava, I., le Roux, S.G., Yadroitsev, I., Fieres, J., Reinhart, C., Rossouw, P., 2017b. Prediction of mechanical performance of Ti6Al4V cast alloy based on microCT-based load simulation. *J. Alloy. Compd.* 724, 267–274.
- Gibson, L.J., Ashby, M.F., 1999. *CellularSolids: Structure and Properties*. Cambridge university press.
- Maskery, I., Aboulkhair, N.T., Aremu, A.O., Tuck, C.J., Ashcroft, I.A., 2017. Compressive failure modes and energy absorption in additively manufactured double gyroid lattices. *Addit. Manuf.* 16, 24–29.
- Naleway, S.E., Porter, M.M., McKittrick, J., A Meyers, M., 2015. Structural design elements in biological materials: application to bioinspiration. *Adv. Mater.* 27, 5455–5476.
- Torres, F.G., Lama, D., 2017. Failure retardation in body armor. *Bioinspired Biomim. Nanobiomaterials* 6, 37–50.
- Wang, B., Yang, W., Sherman, V.R., Meyers, M.A., 2016. Pangolin armor: overlapping, structure, and mechanical properties of the keratinous scales. *Acta Biomater.* 41, 60–74.
- Yang, W., Chen, I.H., McKittrick, J., Meyers, M.A., 2012. Flexible dermal armor in nature. *JOM* 64, 475–485.
- Yang, W., Chen, I.H., Gludovatz, B., Zimmermann, E.A., Ritchie, R.O., Meyers, M.A., 2013. Natural flexible dermal armor. *Adv. Mater.* 25, 31–48.
- Yang, W., Naleway, S.E., Porter, M.M., Meyers, M.A., McKittrick, J., 2015. The armored carapace of the boxfish. *Acta Biomater.* 23, 1–10.